Planktonic encounter rates with non-spherical encounter zones

Andersen, Anders; Dölger, Julia

Published in:
Journal of the Royal Society. Interface

Link to article, DOI:
10.1098/rsif.2019.0398

Publication date:
2019

Document Version
Peer reviewed version

Planktonic encounter rates with non-spherical encounter zones

Anders Andersen and Julia Dölger

Department of Physics and Centre for Ocean Life, Technical University of Denmark, DK-2800 Kgs. Lyngby, Denmark

Date: 27 June 2019

Abstract

We present general formulas for planktonic predator-prey encounter rates with encounter zones of convex shape and randomly moving point-like prey with ballistic motion. When the predator is not moving, we show that the encounter rate is independent of the shape of the encounter zone around it and proportional to the product of the surface area of the encounter zone and the prey speed. In contrast, the shape of the encounter zone plays a role when both the predator and the prey are moving. Slow predator motion results in only a weak increase of the encounter rate relative to the non-motile predator situation, but it may lead to a significant shift in where prey impact the surface of the encounter zone. By analysing disk-like and rod-like encounter zones with lengthwise and sideways motion, respectively, we show that fast predator motion may significantly influence the encounter rate, depending on the shape and the direction of motion of the encounter zone.

1. Introduction

Encounters between individual organisms are essential for predator-prey interactions and mate finding in the planktonic world [1, 2]. Planktonic encounter rates depend on many factors, including the speeds of the organisms, size and shape of the encounter zone, and hydrodynamic effects. In encounter rate models, a spherical encounter zone with an effective size is often assumed [3, 4, 5, 6]. This approach may be inadequate when the encounter zone is highly non-spherical as for ambush-feeding and mechano-sensing larvae and copepods [7, 8, 9, 10, 11], chemical trails [12], the long and slender prey capture structures (haptonema) of haptophytes [13], and the cone-shaped perceptual fields of visual predators [14, 15, 16, 17]. Additionally, the work on non-spherical encounter zones has focused on particular geometries such as cylinders with spherical end caps for which special simplifying assumptions allow modelling [7]. A systematic framework that enables

derivations of easily applicable formulas and general theorems for non-spherical encounter zones therefore appears to be missing in the plankton literature.

Here we present a general approach that takes the shape of the encounter zone around the predator into account, and allows us to determine predator-prey encounter rates when the plankton move ballistically and hydrodynamic interactions are negligible. We restrict our attention to encounter zones with convex shape. As examples, we consider spheroidal, cylindrical, and cone-shaped encounter zones, and throughout we treat the prey as point-like particles that move randomly with equal probability in all directions (figure 1). Our approach builds on determining the encounter rate kernel per unit surface area of the encounter zone, and it therefore allows description of where prey impact the surface of the encounter zone. We have organized our presentation as follows: We derive the general model framework for the encounter rate kernel in the methods section. In the results section, we first consider the encounter rate kernel when the encounter zone is not moving and we then proceed to analyse the more complex situation in which both predator and prey are moving. Throughout the results section we illustrate the general formulas by applying them to real-world cases, including ambush-feeding and mechano-sensing larvae (*Chaoborus trivittatus*), visual predators (fish), ambush-feeding copepods, and prey capturing haptophytes (flagellates). In the discussion section, we discuss the model assumptions, and in the conclusion section, we summarise our main findings.

2. Method

2.1. Ballistic encounter rate model

Predator-prey encounters are quantified by the encounter rate E, i.e., the number of encounters per unit volume per unit time [1, 2]. (Table 1 provides a glossary of symbols.) The key quantity in our analysis is the encounter rate kernel Q that has dimension of volume per unit time and is independent of the concentrations of predators and prey. In general E and Q are related through the expression:

$$E = Q\, C_1\, C_2\,,$$

where C_1 and C_2 denote the concentrations of predators and prey, respectively [1]. We shall describe the encounter zone by its size and shape, and we assume that the encounter zone is moving

with speed v in a direction of motion specified relative to its orientation. We let the encounter zone represent the zone around the predator, on which prey is encountered, i.e., where prey can be directly touched or remotely sensed and thus made available for capture. We disregard size and shape of the prey and treat them as point-like particles that move randomly with speed u and equal probability in all directions. We neglect hydrodynamic interactions and assume that the encounter zones and the prey move ballistically, i.e., with constant speeds along straight paths that are long in comparison with the characteristic length scale L of the encounter zone [2, 18]. For randomly moving prey that move with ballistic runs of run time τ and run length $\lambda = u\,\tau$, and reorient in between consecutive runs, we need $\lambda \gg L$ for the model assumption of straight paths to be applicable. If the run length instead were much smaller than the length scale of the encounter zone, the ballistic approximation would not be applicable, and instead the diffusive approximation would be appropriate [18]. Finally, we assume that the concentrations of predators and prey are uniform, and that any depletion of the prey concentration near the surface of the encounter zone is insignificant. This assumption does in general only hold if the shape of the encounter zone is convex, as we shall return to in the discussion.

2.2. Encounter rate kernel

Encounters occur when prey hit somewhere on the surface of the encounter zone, and mathematically the encounter rate kernel Q is the surface integral of the encounter rate kernel per unit surface area q over the surface of the encounter zone:

$$Q = \int_S q \, \mathrm{d}S \, .$$

The encounter rate kernel per unit surface area has dimension of length per unit time. It varies over the surface when the encounter zone is moving, since q depends on the local orientation of the surface of the encounter zone relative to its direction of motion (figure 2, inset). The encounter rate kernel per unit surface area turns out to have the following form:

$$q = \begin{cases} 0 & \text{if } v_n < -u \\ \frac{1}{4} u \left(1 + \frac{v_n}{u}\right)^2 & \text{if } -u \le v_n < u \\ v_n & \text{if } v_n \ge u \, , \end{cases}$$

where v_n is the outward normal (perpendicular) component of the velocity of the encounter zone (Appendix A). The formula shows that none of the prey immediately outside the encounter zone hit the surface when the encounter zone is moving rapidly away from the prey ($v_n < -u$), whereas all of the prey immediately outside the encounter zone hit the surface when the encounter zone is moving rapidly into the prey ($v_n \geq u$). In the intermediate interval ($-u \leq v_n < u$) the expression for q displays a smooth transition between the two extreme behaviours (figure 2).

3. Results

3.1. Non-motile encounter zone and randomly moving prey

We first consider the encounter situation in which the encounter zone is not moving and the prey move randomly with equal probability in all directions. In this case, q is uniform over the surface of the encounter zone (figure 2), and it is proportional to the prey speed:

$$q = \frac{1}{4}\, u\,.$$

This result is equivalent to the expression for the collision rate of gas molecules with a surface that is derived in the kinetic theory of gasses [19]. Since q is independent of position, the surface integral of q over the surface of the encounter zone simplifies greatly [13]. We find the expression:

$$Q = \frac{1}{4}\, S\, u\,,$$

where S is the surface area of the encounter zone:

$$S = \int_S \mathrm{d}S\,.$$

The formula allows immediate analytical determination of Q for generic shapes such as sphere, cylinder, and spherical cone (table 2), and it reduces the calculation of Q to the calculation of S when the encounter zone is only known empirically. Importantly the formula shows that Q is proportional to S and independent of the shape of the encounter zone.

It follows immediately from the previous analysis that Q is independent of the shape of the encounter zone, whereas this significant fact is not apparent when using the standard approach to

the problem [8]. In the standard approach, one does not need to assume that the encounter zone is convex, and Q is determined as the product of u and the average of the projected area A of the encounter zone. The standard expression for Q is therefore

$$Q = \langle A \rangle \, u \, ,$$

where $\langle A \rangle$ denotes the average of A over all possible directions (Appendix B). By comparing the two expressions for Q we are led to the geometrical identity

$$\langle A \rangle = \frac{1}{4} \, S \, .$$

This remarkable relation between the average projected area and the surface area is valid when the shape of the encounter zone is convex, and it is known in mathematics as Cauchy's surface area theorem [20, 21]. The two expressions for Q are therefore equivalent when the shape of the encounter zone is convex. Direct calculation of the average projected area of an encounter zone is typically tedious, and the expression for Q in terms of S is often the easiest to work with.

To illustrate the use of the general formula to real-world cases we consider two examples involving planktonic larvae and visual predators, respectively. We can model the ambush-feeding and mechano-sensing larvae *Chaoborus trivittatus* that feeds on swimming copepods ($u = 1.5 \text{ mm s}^{-1}$) as a non-motile, cylindrical encounter zone ($H = 13.2 \text{ mm}$ and $R = 2.4 \text{ mm}$) without and with spherical end caps [7]. For the cylindrical encounter zone without spherical end caps (table 2), we find the encounter rate kernel: $Q = (1/2) \, \pi \, (H + R) \, R \, u = 88 \text{ mm}^3\text{s}^{-1}$, and for the cylindrical encounter zone with spherical end caps, we correspondingly find the larger value: $Q = (1/4) \, S \, u = (1/2) \, \pi \, (H + 2 \, R) \, R \, u = 102 \text{ mm}^3\text{s}^{-1}$ due to the larger surface area of the encounter zone. As a second example, we consider a cone-shaped encounter zone ($a = 100 \text{ cm}$ and $\gamma = 45 \text{ deg}$) to represent the visual field of a fish of size 1 cm that feeds on prey of size 1 mm [17]. If we assume that the fish is not moving and encounters motile prey ($u = 1.0 \text{ cm s}^{-1}$), we estimate the encounter rate kernel: $Q = (1/4) \, \pi \, a^2 \, (2 - 2 \cos\gamma + \sin\gamma) \, u = 1.0 \cdot 10^4 \text{ cm}^3\text{s}^{-1}$ (table 2). This example illustrates the simple use of the general formula to an encounter zone that would be difficult to work with analytically using the standard approach.

3.2. Moving spherical encounter zone and randomly moving prey

The encounter rate kernel is well-known for a spherical encounter zone when both the encounter zone and the prey are moving [3, 19]. With our approach the expression for Q can be obtained by direct evaluation of the integral of q over the surface of the encounter zone. The result becomes:

$$\frac{Q}{\pi\, a^2\, u} = \begin{cases} 1 + \frac{1}{3}\left(\frac{v}{u}\right)^2 & \text{if } v < u \\ \frac{u}{3\, v} + \frac{v}{u} & \text{if } v \geq u\,, \end{cases}$$

where a is the radius of the encounter zone, and we have normalized Q with the encounter rate kernel $(1/4)\, S\, u = \pi\, a^2\, u$ for the non-motile encounter zone (figure 3). The motion of the encounter zone leads to a weak increase of Q when $v < u$ [2], but this does not mean that the motion of the encounter zone does not strongly influence the encounter situation. To illustrate this effect we show q/u as function of the angle ψ between the outward normal to the surface of the encounter zone and its direction of motion. The encounter rate kernel per unit surface area changes from being uniform when $v = 0$ to being high on the front half of the encounter zone ($\psi < 90$ deg) and low on the back half of the encounter zone ($\psi > 90$ deg) when $v = u$ (figure 4). To quantify the effect when $v < u$ we determine the encounter rate kernel for the encounters on the front half of the encounter zone:

$$\frac{Q_{\text{front}}}{\pi\, a^2\, u} = \frac{1}{2}\left[1 + \frac{v}{u} + \frac{1}{3}\left(\frac{v}{u}\right)^2\right],$$

and the encounter rate kernel for the encounters on the back half of the encounter zone:

$$\frac{Q_{\text{back}}}{\pi\, a^2\, u} = \frac{1}{2}\left[1 - \frac{v}{u} + \frac{1}{3}\left(\frac{v}{u}\right)^2\right].$$

Interestingly, the two expressions contain linear v/u terms with opposite signs. The strong linear terms are of similar magnitude and they therefore cancel out in the expression for the total encounter rate kernel ($Q = Q_{\text{front}} + Q_{\text{back}}$) and leave only a weak quadratic $(v/u)^2$ term. However, the strong linear terms dominate the increase of Q_{front} and the decrease of Q_{back}, and they explain the significant shift from back to front of where prey impact the encounter zone (figure 4).

3.3. The effects of the shape of the encounter zone

The shape and the direction of motion of a moving non-spherical encounter zone influence the encounter rate kernel, and the situation is particularly complex when both the encounter zone and the prey are moving. To show the key effects qualitatively, we consider the encounter rate kernel per unit surface area for disk-shaped (oblate) and rod-shaped (prolate) spheroidal encounter zones that are moving lengthwise (figure 5). Both disk-shaped and rod-shaped encounter zones experience an increase of q on the front half and a decrease of q on the back half due to the motion of the encounter zone, but the effect on the encounter rate kernel Q is strong and important for flat disks whereas it is weak and insignificant for slender rods.

To explore the problem quantitatively, we first consider the situation in which the encounter zone is moving slower than the prey. Assuming that $v < u$ we find the general encounter rate kernel:

$$Q = \frac{1}{4}\, S\, u \left[1 + 2\,\alpha\,\frac{v}{u} + \beta \left(\frac{v}{u}\right)^2\right],$$

where we have defined two geometrical shape parameters for the encounter zone:

$$\alpha = \frac{1}{S}\int_S \cos\psi \;\mathrm{d}S\,,$$
$$\beta = \frac{1}{S}\int_S \cos^2\psi \;\mathrm{d}S\,.$$

The expression for Q holds for both open and closed surfaces, and the two geometrical shape parameters satisfy the general constraints:

$$-1 \le \alpha \le 1\,,$$
$$0 \le \beta \le 1\,.$$

For closed surfaces, the linear α-term vanishes as can be shown using Gauss' theorem, and irrespective of the shape of the encounter zone only the quadratic β-term remains in the expression for the encounter rate kernel:

$$Q = \frac{1}{4}\, S\, u \left[1 + \beta \left(\frac{v}{u}\right)^2\right].$$

We immediately notice that the expression reduces to the expression for Q with a non-motile encounter zone and randomly moving prey when $v = 0$. In addition, the expression for a spherical encounter zone with radius a is a special case with $S = 4\,\pi\,a^2$ and $\beta = 1/3$ (table 3).

To further illustrate the dependence of the parameter β on the geometrical shape and the direction of motion of the encounter zone, we consider cylindrical encounter zones with lengthwise and sideways motion, respectively, and different aspect ratio, i.e., ratio between height H and radius R. For a cylindrical encounter zone that is moving lengthwise with $v < u$ we use the formula derived above (table 3). When $v \geq u$ we have at the front surface $v_n = v$ and thus $v_n \geq u$ and $q = v$, at the lateral surface $v_n = 0$ and thus $q = (1/4)\,u$, and at the back surface $v_n = -v$ and thus $v_n \leq -u$ and $q = 0$. In total, we find for a cylindrical encounter zone with lengthwise motion:

$$\frac{Q}{(1/4)\,S\,u} = \begin{cases} 1 + \beta\left(\frac{v}{u}\right)^2 & \text{if } v < u \\ 1 - \beta + 2\,\beta\frac{v}{u} & \text{if } v \geq u\,, \end{cases}$$

where $S = 2\,\pi\,(H + R)\,R$ and $\beta = R/(H + R)$. We see that lengthwise motion of a disk-shaped encounter zone ($H \ll R$) leads to a strong ($\beta \approx 1$) increase of Q, whereas it for a rod-shaped encounter zone ($H \gg R$) only leads to a weak ($\beta \approx 0$) increase of Q (figure 6a). In contrast we observe a qualitatively reverse scenario when a cylindrical encounter zone is moving sideways, i.e., $\beta \approx 0$ if $H \ll R$ and $\beta \approx 1/2$ if $H \gg R$ (table 3 and figure 6b).

An instructive example is provided by the ambush-feeding copepod *Oithona similis* that uses its mechano-sensing antennae to perceive motile prey [8]. We treat the antennae as a cylindrical encounter zone ($H = 1.0\ \mathrm{mm}$ and $R = 0.14\ \mathrm{mm}$) that moves sideways with the sinking speed of the copepod ($v = 0.09\ \mathrm{mm\,s^{-1}}$), and we consider the motile ($u = 0.37\ \mathrm{mm\,s^{-1}}$) dinoflagellate *Gymnodinium dominans* as prey [8]. We find the value: $Q = (1/4)\,S\,u\,[1 + \beta(v/u)^2] = 0.095\ \mathrm{mm^3 s^{-1}}$, where we have used S and β for a cylindrical encounter zone that moves sideways with $v < u$ (table 3). We note that the slow sinking motion of the copepod increases the encounter rate kernel insignificantly from the value: $Q = (1/4)\,S\,u\ = 0.093\ \mathrm{mm^3 s^{-1}}$ that we would estimate if the copepod were not moving.

Estimation of the encounter rate kernel for the capture of motile, bacteria-sized prey on the capture-structure (haptonema) of the haptophyte *Prymnesium polylepis* provides a final example. We model the encounter zone around the haptonema as cylindrical with radius equal to the (negligible) radius of the haptonema plus the radius of the spherical prey ($H = 13.5$ μm and $R = 0.85$ μm). We assume that the haptonema is moving lengthwise with speed equal to the swimming speed of the haptophyte ($v = 45$ μm s^{-1}), and we consider motile, bacteria-sized prey with run-tumble motion and run length longer than the haptonema ($u = 32$ μm s^{-1} and $\lambda = 46$ μm) [13]. Using the formula for a cylindrical encounter zone with lengthwise motion we find the encounter rate kernel: $Q = 679$ $\mu\mathrm{m}^3\mathrm{s}^{-1}$, whereas we estimate the value: $Q = 613$ $\mu\mathrm{m}^3\mathrm{s}^{-1}$ if we disregard the swimming of the haptophyte [13]. We see that the swimming of the haptophyte increases the encounter rate kernel by only a small fraction as expected since the slender, cylindrical encounter zone is moving lengthwise.

4. Discussion

When applying the encounter rate expressions to concrete problems, one should keep in mind that hydrodynamic effects were disregarded in their derivations. Two types of hydrodynamic effects that are difficult to describe in simple models affect encounter rates. Firstly, low Reynolds number flows at the planktonic microscale lead to repulsive disturbances that hinder direct predator-prey contact [2, 22, 23], and secondly small-scale turbulent flows in the aquatic environments may facilitate predator-prey encounters, but also sometimes make the prey more difficult to catch [24, 5, 11]. Repulsive disturbances are of significance, e.g., when prey are caught by direct impact on the cell of the predator, and they can be disregarded when the encounter zone is a chemical trail or the cone-shaped encounter zone of a visual predator.

In all of our derivations, except the derivation of the expression $Q = \langle A \rangle\, u$, we considered convex encounter zones. To illustrate the importance of this assumption, let us compare the results for a cylindrical (convex) encounter zone and a non-convex encounter zone in the shape of a cylindrical and thin-walled tube. We assume that the two encounter zones have the same height H and outer radius R and that they are slender with $H \gg R$. When the encounter zones are not moving and the prey move randomly, the expression $Q = \langle A \rangle\, u$ correctly predicts $Q \approx (1/2)\, \pi\, H\, R\, u$ in both cases, since the average projected areas are approximately the same (Appendix B). For the convex cylinder,

the expression $Q = (1/4)\, S\, u$ also correctly predicts Q, but the expression wrongly overestimates Q by a factor of approximately two for the non-convex tube, since its surface area is approximately twice as large as the surface area of the cylinder. The problem is that depletion of the prey concentration near the surface of the encounter zone is assumed insignificant in our approach. This assumption is not satisfied on the inside of the non-convex tube that is shielded from the outside ballistic prey motion, but it is applicable for the convex cylinder.

5. Conclusion

Building on the expression for the encounter rate kernel per unit surface area of the encounter zone, we have generalized the well-known expression for the encounter rate for a spherical encounter zone when both the encounter zone and the prey are moving. The general expressions are applicable to estimate encounter rates in concrete predator-prey encounter situations as we have illustrated in the four examples with different types of plankton, and they provide tools to make strong and testable predictions about the influence of the motion and the shape of the encounter zone. We have derived two main quantitative predictions. Firstly, we have shown that the encounter rate is proportional to the surface area of the encounter zone ($Q = (1/4)\, S\, u$) and independent of its shape when the encounter zone is not moving. Secondly, we have shown how the encounter rate depends on the direction of motion and the shape of the encounter zone when it is non-spherical and in motion, and we have demonstrated that this dependence can be significant (figures 5 and 6). We hope that our predictions will be tested in future studies, both numerically to quantify the effects of our simplifying assumptions and against laboratory data on predator-prey encounter rates for planktonic organisms in different encounter situations.

Appendices

Appendix A. Derivation of the encounter rate kernel per unit surface area

To derive the expression for the encounter rate kernel per unit surface area:

$$q = \begin{cases} 0 & \text{if } v_n < -u \\ \frac{1}{4} u \left(1 + \frac{v_n}{u}\right)^2 & \text{if } -u \le v_n < u \\ v_n & \text{if } v_n \ge u\,, \end{cases}$$

we look locally at the surface of the encounter zone. The outward normal component of the velocity of the encounter zone is by definition

$$v_n = \vec{v} \cdot \vec{n} \,,$$

where $\vec{v}$ is the velocity of the encounter zone and $\vec{n}$ the outward unit normal. When $v_n < -u$ the surface is moving inwards so rapidly that none of the prey immediately outside hit it, whereas when $v_n \geq u$ the surface is moving outwards so rapidly that all of the prey immediately outside are swept in and $q = v_n$. To derive the expression in the intermediate interval $-u \leq v_n < u$, we choose spherical polar coordinates with the polar axis in the direction of the inward normal, and we let θ denote the polar angle and φ the azimuthal angle. We use the angles to describe the direction of motion of the prey, and we write the inward normal component of the velocity of the prey relative to the surface:

$$w = v_n + u \cos\theta \,.$$

The probability that the prey has directions of motion within the solid angle $\mathrm{d}\Omega$ is $\mathrm{d}\Omega/(4\,\pi)$. To determine q we use $\mathrm{d}\Omega = \sin\theta \,\mathrm{d}\theta \,\mathrm{d}\varphi$ and integrate w over all the directions of motion for which the prey approach the surface. We find that:

$$q = \frac{1}{4\,\pi} \int_0^{\chi} \mathrm{d}\theta \int_0^{2\,\pi} (v_n + u\cos\theta) \sin\theta \,\mathrm{d}\varphi = \frac{1}{4} u \left(1 + \frac{v_n}{u}\right)^2 \,,$$

where the limiting angle χ is determined by the ratio between v_n and u:

$$\cos\chi = -\frac{v_n}{u} \,.$$

In the kinetic theory of gases, q is derived along the same principles to determine the collision rate of gas molecules with a surface in the special case with $v_n = 0$ [19].

Appendix B: Alternative derivation of the encounter rate kernel with a non-motile encounter zone

When the encounter zone is not moving and the prey are moving randomly with equal probability in all directions, we can express Q using the alternative expression:

$$Q = \langle A \rangle \, u \,,$$

where $\langle A \rangle$ denotes the average projected area (silhouette) of the encounter zone with the average extending over all the possible directions:

$$\langle A \rangle = \frac{1}{4\,\pi} \int_0^{\pi} \mathrm{d}\theta \int_0^{2\,\pi} A(\theta, \varphi)\, \sin\theta\, \mathrm{d}\varphi\,.$$

When the run length of the prey $\lambda = u\,\tau$ is large in comparison with the characteristic length scale L of the encounter zone, we can express Q as an integral over the spherical volume with radius λ from which the prey can hit the encounter zone during a time-interval equal to the run time:

$$Q = \frac{1}{\tau} \int_0^{\pi} \mathrm{d}\theta \int_0^{2\,\pi} \sin\theta\, \mathrm{d}\varphi \int_0^{\lambda} p(r, \theta, \varphi)\, r^2 \mathrm{d}r\,.$$

We write the integral using spherical polar coordinates with the origin at the geometric centre of the encounter zone, and we let $p(r, \theta, \varphi)$ denote the probability for a prey with coordinates r, θ, and φ to hit the encounter zone during a time-interval equal to the run time. We can write

$$p(r, \theta, \varphi) = \frac{A(\theta, \varphi)}{4\,\pi\, r^2},$$

where $A(\theta, \varphi)$ is the projected area of the encounter zone. From the integral, we should strictly speaking exclude the region of the encounter zone and extend the outer boundary of the integral correspondingly. Also, the above expression for p is in general invalid for prey near the encounter zone. However, the contributions from these corrections are insignificant when $\lambda \gg L$ and the prey concentration is uniform. The expression for the encounter rate kernel is therefore

$$Q = \frac{1}{4\,\pi\,\tau} \int_0^{\pi} \mathrm{d}\theta \int_0^{2\,\pi} A(\theta, \varphi)\, \sin\theta\, \mathrm{d}\varphi \int_0^{\lambda} \mathrm{d}r = \langle A \rangle\, \frac{\lambda}{\tau}\,,$$

from which the formula $Q = \langle A \rangle\, u$ immediately follows.

As an example, we consider a cylindrical encounter zone with height H and radius R with the assumption that the cylinder is slender ($H \gg R$). We choose a spherical polar coordinate system with origin at the geometric centre of the cylinder, and oriented so that the polar axis is aligned with the axis of the cylinder. Seen from a point with coordinates r, θ, and φ, the cylinder appears with a

projected area that is independent of the azimuthal angle φ and depends only on the polar angle θ. The projected area of the cylinder is

$$A \approx 2\, H\, R \sin\theta\,,$$

and for the average projected area we find

$$\langle A \rangle \approx H\, R \int_0^{\pi} \sin^2\theta \, \mathrm{d}\theta = \frac{1}{2}\, \pi\, H\, R\,.$$

For the encounter rate kernel, we therefore obtain the expression:

$$Q \approx \frac{1}{2} \pi\, H\, R\, u\,.$$

Since the cylindrical encounter zone is convex, the expression corresponds to the formula obtained from the expression for Q in terms of S with $H \gg R$ (table 2).

Authors' contributions

A. A. and J. D. designed and performed the research and wrote the paper.

Competing interests

We have no competing interests.

Acknowledgements

We are grateful to Thomas Kiørboe and Mads Rode for helpful comments on the manuscript.

Funding

This work was supported by the Villum Foundation through the Centre for Ocean Life and by The Independent Research Fund Denmark (grant number 7014-00033B).

References

[1] T. Kiørboe, A Mechanistic Approach to Plankton Ecology, Princeton, New Jersey: Princeton University Press, 2008.

[2] D. B. Dusenbery, Living at Micro Scale, Cambridge, Massachusetts: Harvard University Press, 2009.

[3] J. Gerritsen and J. R. Strickler, "Encounter Probabilities and Community Structure in Zooplankton: a Mathematical Model," *Journal of the Fisheries Research Board of Canada,* vol. 34, p. 73–82, 1977.

[4] A. R. Paradis, M. Pépin and P. Pepin, "Disentangling the effects of size-dependent encounter and susceptibility to predation with an individual-based model for fish larvae," *Canadian Journal of Fisheries and Aquatic Sciences,* vol. 56, p. 1562–1575, 1999.

[5] D. M. Lewis and T. J. Pedley, "Planktonic Contact Rates in Homogeneous Isotropic Turbulence: Theoretical Predictions and Kinematic Simulations," *Journal of Theoretical Biology,* vol. 205, p. 377–408, 2000.

[6] M. Uttieri, D. Cianelli and E. Zambianchi, "Behaviour-dependent predation risk in swimming zooplankters," *Zoological Studies,* vol. 52, pp. number 32, 11 pages, 2013.

[7] L. A. Giguère, A. Delâge, L. M. Dill and J. Gerritsen, "Predicting encounter rates for zooplankton: a model assuming a cylindrical encounter field," *Canadian Journal of Fisheries and Aquatic Sciences,* vol. 39, p. 237–242, 1982.

[8] C. Svensen and T. Kiørboe, "Remote prey detection in Oithona similis: hydromechanical versus chemical cues," *Journal of Plankton Research,* vol. 22, p. 1155–1166, 2000.

[9] S. Lapesa, T. W. Snell, D. M. Fields and M. Serra, "Predatory interactions between a cyclopoid copepod and three sibling rotifer species," *Freshwater Biology,* vol. 47, p. 1685–1695, 2002.

[10] D. M. Lewis, "Planktonic encounter rates in homogeneous isotropic turbulence: The case of predators with limited fields of sensory perception," *Journal of Theoretical Biology,* vol. 222, p. 73–97, 2003.

[11] H. L. Pécseli, J. K. Trulsen and Ø. Fiksen, "Predator–prey encounter and capture rates for plankton in turbulent environments," *Progress in Oceanography,* vol. 85, pp. 171-179, 2010.

[12] T. Kiørboe, "Attack or Attacked: The Sensory and Fluid Mechanical Constraints of Copepods' Predator–Prey Interactions," *Integrative and Comparative Biology,* vol. 53, p. 821–831, 2013.

[13] J. Dölger, L. T. Nielsen, T. Kiørboe and A. Andersen, "Swimming and feeding of mixotrophic biflagellates," *Scientific Reports,* vol. 7, pp. number 39892, 10 pages, 2017.

[14] C. Luecke and W. J. O'Brien, "Prey Location Volume of a Planktivorous Fish: A New Measure of Prey Vulnerability," *Canadian Journal of Fisheries and Aquatic Sciences,* vol. 38, pp. 1264-1270, 1981.

[15] R. L. Dunbrack and L. M. Dill, "Three-Dimensional Prey Reaction Field of the Juvenile Coho Salmon (Oncorhynchus kisutch)," *Canadian Journal of Fisheries and Aquatic Sciences,* vol. 41, p. 1176–1182, 1984.

[16] H. I. Browman and W. J. O'Brien, "Foraging and prey search behaviour of golden shiner (Notemigonus crysoleucas) larvae," *Canadian Journal of Fisheries and Aquatic Sciences,* vol. 49, p. 813–819, 1992.

[17] D. L. Aksnes and J. Giske, "A theoretical model of aquatic visual feeding," *Ecological Modelling,* vol. 67, p. 233–250, 1993.

[18] A. W. Visser and T. Kiørboe, "Plankton motility patterns and encounter rates," *Oecologia,* vol. 148, pp. 538-546, 2006.

[19] W. Kauzmann, Kinetic Theory of Gases, New York: W. A. Benjamin, Inc., 1966.

[20] V. Vouk, "Projected Area of Convex Bodies," *Nature,* vol. 162, pp. 330-331, 1948.

[21] A. R. G. Lang, "Application of some of Cauchy's theorems to estimation of surface areas of leaves, needles and branches of plants, and light transmittance," *Agricultural and Forest Meteorology,* vol. 55, pp. 191-212, 1991.

[22] T. Kiørboe, "Fluid dynamic constraints on resource acquisition in small pelagic organisms," *The European Physical Journal Special Topics,* vol. 225, p. 669–683, 2016.

[23] M. Jabbarzadeh and H. C. Fu, "Viscous constraints on microorganism approach and interaction," *Journal of Fluid Mechanics,* vol. 851, pp. 715-738, 2018.

[24] B. J. Rothschild and T. R. Osborn, "Small-scale turbulence and plankton contact rates," *Journal of Plankton Research,* vol. 10, pp. 465-474, 1988.

TABLES AND TABLE CAPTIONS

Table 1. Glossary of symbols.

Symbol	Description
a	Radius of sphere and spherical cone
A	Projected area of encounter zone
C	Concentration, number of organisms per unit volume
E	Encounter rate, number of encounters per unit volume per unit time
H	Height of cylindrical encounter zone
L	Characteristic length scale of encounter zone
q	Encounter rate kernel per unit surface area
Q	Encounter rate kernel, volume per unit time
R	Radius of cylindrical encounter zone
S	Surface area of encounter zone
u	Speed of prey
v	Speed of predator (encounter zone)
α	Geometrical shape parameter, linear term
β	Geometrical shape parameter, quadratic term
γ	Half cone angle of spherical cone
θ	Polar angle, spherical polar coordinates
λ	Run length of prey
τ	Run time of prey
φ	Azimuthal angle, spherical polar coordinates
χ	Angle used in encounter rate derivations
ψ	Angle between predator velocity and encounter surface normal

Table 2. Encounter rate kernel for non-motile encounter zones with different shape.

Encounter zone	Encounter rate kernel Q
Sphere	$\pi\, a^2\, u$
Cylinder	$\frac{1}{2}\, \pi\, (H + R)\, R\, u$
Spherical cone	$\frac{1}{4}\, \pi\, a^2\, (2 - 2\cos\gamma + \sin\gamma)\, u$

Table 3. Encounter rate parameters for closed encounter zones with different shape and different direction of motion. We assume that the encounter zones move slower than the prey ($v < u$).

Encounter zone	Surface area S	Direction of motion	Geometrical shape parameter β
Sphere	$4\, \pi\, a^2$	Arbitrary	$\frac{1}{3}$
Cylinder	$2\, \pi\, (H + R)\, R$	Lengthwise	$\frac{R}{H + R}$
		Sideways	$\frac{H}{2\, (H + R)}$

FIGURES

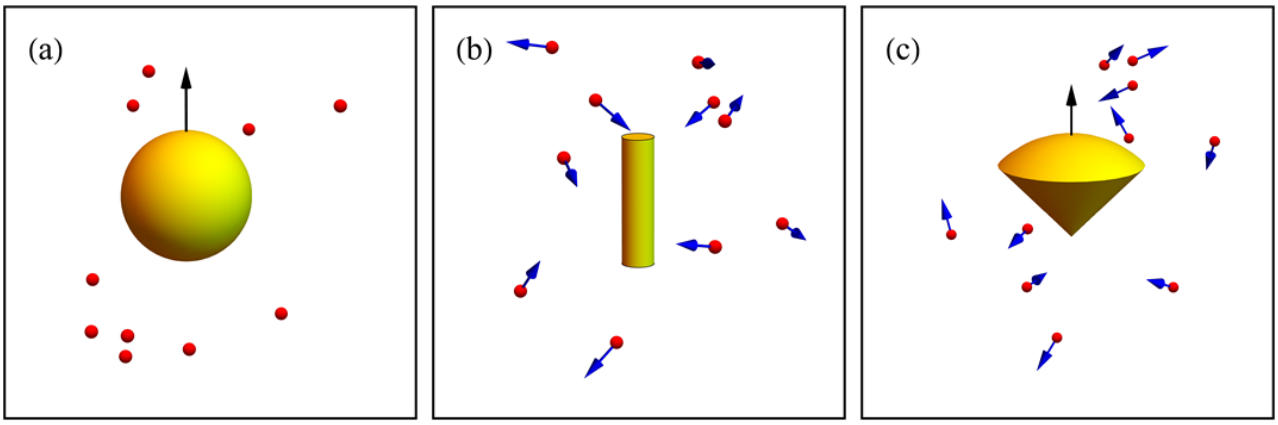

Figure 1. Examples of different encounter zones and situations. (a) Moving, spherical encounter zone and non-motile prey, (b) non-motile, cylindrical encounter zone and randomly moving prey, and (c) moving, cone-shaped encounter zone (spherical cone) and randomly moving prey. The black vectors show the velocities of the encounter zones (yellow) and the blue vectors the velocities of the small and randomly moving prey (red spheres). The three-dimensional positions of the prey are random, and the directions of motion of the prey are random with equal probability in all directions.

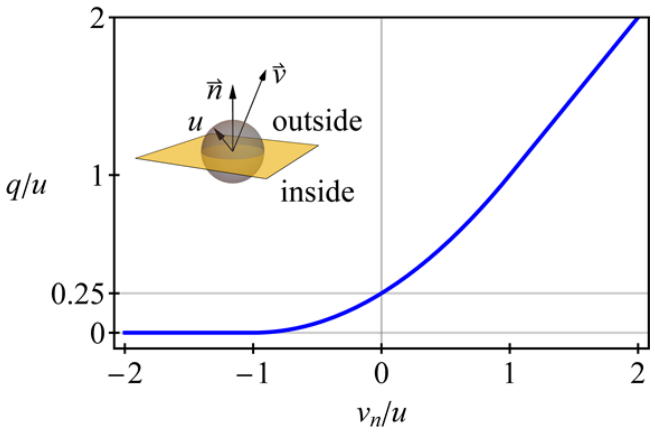

Figure 2. Encounter rate kernel per unit surface area as function of the outward normal component of the velocity of the encounter zone. The inset shows the local geometry at the surface (yellow) of the encounter zone with $\vec{v}$ indicating the velocity of the encounter zone and $\vec{n}$ the outward unit normal. The descriptions "inside" and "outside" refer to the regions inside and outside of the encounter zone, respectively. All the prey are moving with speed u and the directions of motion of the prey are random and with equal probability in all directions as indicated by the grey sphere. (The radius of the sphere indicates the speed u that is common to all prey.) The encounter rate kernel per unit surface area q and the outward normal component of the velocity of the encounter zone $v_n = \vec{v} \cdot \vec{n}$ are both normalized by the prey speed u. We find that $q/u = 0.25$ (horizontal line) when $v_n = 0$. None of the prey immediately outside the encounter zone hit the surface ($q = 0$) when $v_n < -u$, whereas all of the prey immediately outside hit the surface ($q = v_n$) when $v_n \geq u$.

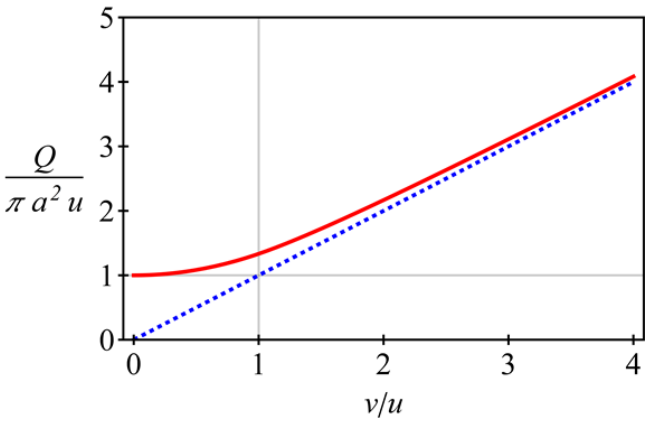

Figure 3. Encounter rate kernel for a moving spherical encounter zone and randomly moving prey. The encounter rate kernel Q (solid line, red) is shown as function of the ratio between the encounter zone speed v and the prey speed u, and it is normalized by the encounter rate kernel $(1/4)\ S\ u = \pi\ a^2\ u$ for the non-motile, spherical encounter zone. The motion of the encounter zone leads to an insignificant increase of Q when $v < u$, but the increase of Q due to the motion of the encounter zone is significant when $v \geq u$. The linear approximation (dashed line, blue) is valid when the motion of the encounter zone dominates and the motion of the prey is negligible.

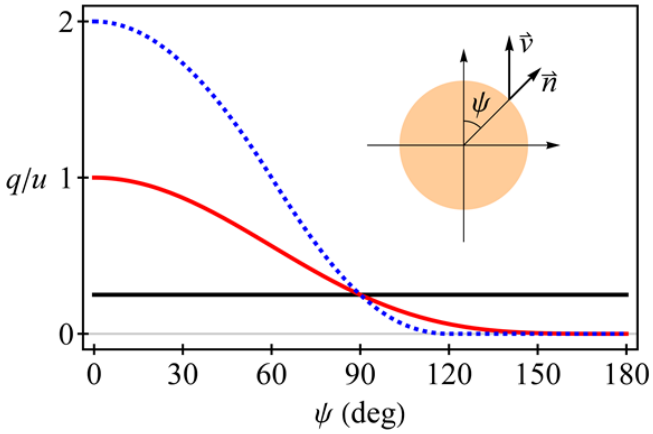

Figure 4. Encounter rate kernel per unit surface area as function of the position on the surface of a spherical encounter zone. Non-motile encounter zone ($v = 0$) and prey moving randomly with speed u (solid line, black), both encounter zone and prey in motion with $v = u$ (solid line, red), and both encounter zone and prey in motion with $v = 2\,u$ (dashed line, blue). The inset shows the velocity of the encounter zone $\vec{v}$ and the outward unit normal $\vec{n}$ at the angular position ψ. The motion of the encounter zone enhances q on the front half and reduces q to basically zero on the back half.

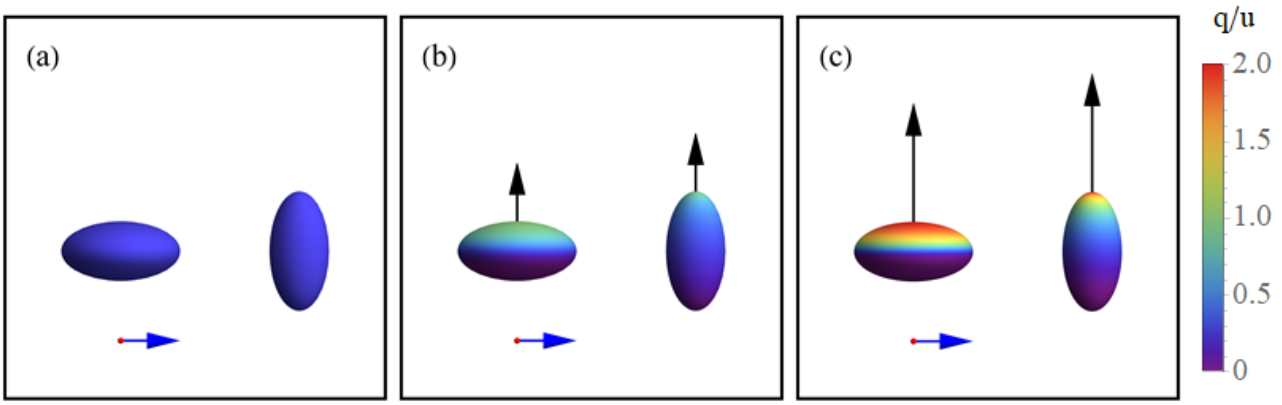

Figure 5. Encounter rate kernel per unit surface area for two differently shaped spheroidal encounter zones that are moving lengthwise. Disk-shaped zones with ratio 1/2 between polar radius and equatorial radius (left) and rod-shaped zones with ratio 2 between polar radius and equatorial radius (right). (a) Non-motile encounter zones ($v = 0$) and prey moving randomly with speed u, (b) both encounter zones and prey in motion ($v = u$), and (c) both encounter zones and prey in motion ($v = 2\,u$). The black vectors indicate the velocities of the encounter zones, the blue vectors the prey speed, and the surface colour plots the encounter rate kernel per unit surface area q normalized by u. The disk-shaped zone experiences a strong increase of q on the front-half due to its motion, whereas the rod-shaped zone only experiences an increase of q near the foremost point.

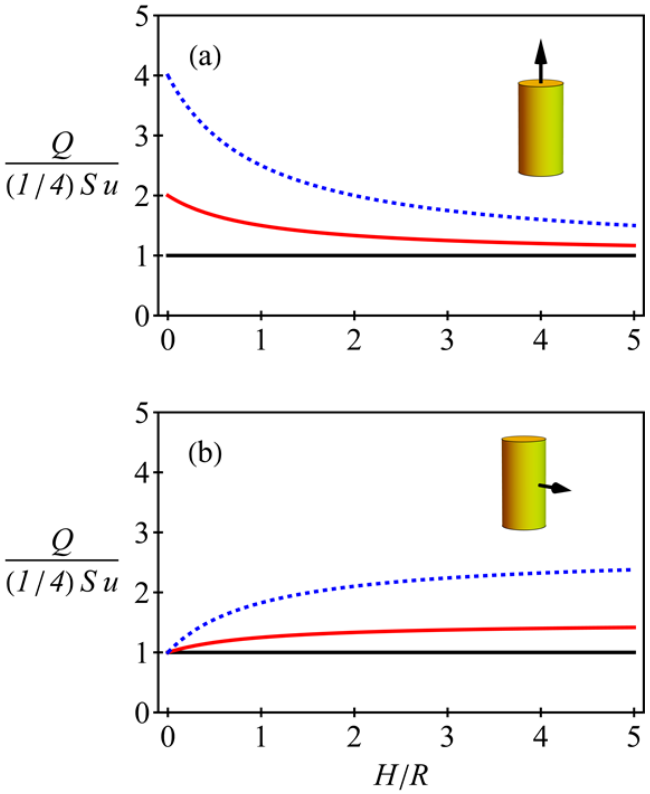

Figure 6. Encounter rate kernel for cylindrical encounter zones with different aspect ratio. The insets show the directions of motion of the encounter zones: (a) lengthwise and (b) sideways. The encounter rate kernel Q is normalized by the encounter rate kernel $(1/4)\ S\ u$ for the corresponding non-motile encounter zone, and it is shown as function of the aspect ratio H/R. Non-motile encounter zone ($v = 0$) and prey moving randomly with speed u (solid line, black), both encounter zone and prey in motion with $v = u$ (solid line, red), and both encounter zone and prey in motion with $v = 2\ u$ (dashed line, blue). Lengthwise motion leads to a strong increase of Q for disk-shaped ($H/R \ll 1$) encounter zones, whereas sideways motion leads to a strong increase of Q for rod-shaped ($H/R \gg 1$) encounter zones.